Full wave simulations of fast wave heating losses in the scrape-off layer of NSTX and NSTX-U

2014 Nucl. Fusion 54 083004

(http://iopscience.iop.org/0029-5515/54/8/083004)

IOP Publishing | International Atomic Energy Agency Nuclear Fusion
Nucl. Fusion **54** (2014) 083004 (6pp) doi:10.1088/0029-5515/54/8/083004

Full wave simulations of fast wave heating losses in the scrape-off layer of NSTX and NSTX-U

N. Bertelli[1], E.F. Jaeger[2], J.C. Hosea[1], C.K. Phillips[1], L. Berry[3], S.P. Gerhardt[1], D. Green[3], B. LeBlanc[1], R.J. Perkins[1], P.M. Ryan[3], G. Taylor[1], E.J. Valeo[1] and J.R. Wilson[1]

[1] Princeton Plasma Physics Laboratory, Princeton, New Jersey 08543, USA
[2] XCEL Engineering Inc, 1066 Commerce Park Drive, Oak Ridge, Tennessee 37830, USA
[3] Oak Ridge National Laboratory, PO Box 2008, Oak Ridge, Tennessee 37831-6169, USA

E-mail: nbertell@pppl.gov

Received 18 March 2014, revised 18 April 2014
Accepted for publication 25 April 2014
Published 21 May 2014

Abstract

Full wave simulations of fusion plasmas show a direct correlation between the location of the fast-wave cut-off, radiofrequency (RF) field amplitude in the scrape-off layer (SOL) and the RF power losses in the SOL observed in the National Spherical Torus eXperiment (NSTX). In particular, the RF power losses in the SOL increase significantly when the launched waves transition from evanescent to propagating in that region. Subsequently, a large amplitude electric field occurs in the SOL, driving RF power losses when a proxy collisional loss term is added. A 3D reconstruction of absorbed power in the SOL is presented showing agreement with the RF experiments in NSTX. Loss predictions for the future experiment NSTX-Upgrade (NSTX-U) are also obtained and discussed.

Keywords: fast wave, heating losses, scrape-off layer

(Some figures may appear in colour only in the online journal)

1. Introduction

The ability of externally applied auxiliary heating power using radio-frequency (RF) waves to sustain and control the plasma performance has been demonstrated on numerous tokamak devices over the past half century. However, essentially all of these experiments have found that up to 50% or more of the launched RF power can be lost in the region outside of the last closed flux surface (LCFS), thereby degrading the efficiency of RF heating and profile control within the main body of the plasma. Recent experimental studies of high harmonic fast wave (HHFW) heating on the National Spherical Torus eXperiment (NSTX) [1] have demonstrated that substantial HHFW power loss (up to 60% of the coupled HHFW power can be lost) can occur along the open field lines in the scrape-off layer (SOL) (i.e., the region of the plasma between LCFS and tokamak vessel, where the magnetic field lines are open and the plasma density has a sharp profile) when edge densities are high enough that the fast waves can propagate close to the launcher [2–6]. In addition, experimental measurements of RF power losses have been found in different machines, with a focus on erosion and impurity generation [7, 8]. These large RF power losses in the SOL can have a significant impact on the performance of the ion cyclotron range of frequency (ICRF) system in the current experiments and may be particularly problematic for the long pulse plasmas anticipated in the ITER experiment. For several decades, RF modelling codes have neglected the presence of the SOL, concentrating instead on understanding the wave dynamics in the core plasma bounded by the LCFS. More recently, some RF codes, such as the full wave code AORSA [9], have been improved to include the edge plasma beyond the LCFS [10]. Although several possible physical mechanisms behind the interaction between RF waves and the SOL have been studied (parametric decay [11], sheath effects [12], coaxial modes [10], etc.) a clear explanation of RF power losses in this region is still missing. In this paper we demonstrate for the first time a direct correlation between the location of the fast wave cut-off layer relative to the antenna and the LCFS, the large amplitude of the RF fields in the scrape-off region, and the power losses in the SOL (driven by the RF field) observed in the NSTX experiments by making use of the full wave simulations. In particular, a strong transition to higher SOL power losses has been found when the fast wave (FW) cut-off is removed from in front of the antenna with increasing edge density, consistent with the experimental observations [3]. More generally, when evanescent waves become propagating waves in the SOL, due to higher density in front of the antenna, the power losses in the SOL start to

increase significantly, commensurate with the amplitude of the RF field found in the SOL. The full 3D power absorption reconstructions show that the absorbed power in the SOL is larger near the LCFS and near the front of the antenna, as experimentally observed. Finally, the full wave simulations based on this model predict that plasmas in NSTX-Upgrade (NSTX-U) will have a wider operating SOL density range in which the RF power losses in the SOL will be low.

2. Numerical results

In these numerical studies we make use of the full wave code AORSA that solves the Helmholtz wave equation for a tokamak geometry, including the SOL region beyond the LCFS where the magnetic field lines are open [9, 10]. AORSA includes the complete non-local, integral operator for the dielectric tensor that is valid for 'all orders', by taking into account all contributions in $k_\perp \rho_i$ ($k_\perp$, ρ_i are the perpendicular component of the wave vector relative to the local equilibrium magnetic field and the ion Larmor radius, respectively). This is essential for NSTX HHFW in which the ion Larmor radius is larger than the perpendicular wavelength and the ion-cyclotron harmonic number is large. AORSA utilizes a Fourier decomposition in the Cartesian coordinates x and y (in the poloidal plane) and in the toroidal direction of symmetry (ϕ), $e^{in_\phi \phi}$ (n_ϕ is the toroidal mode number). The density profile in the SOL is described by an exponential decay from the LCFS and a minimum density in front of the antenna, n_{ant}, as a function of the square root of the normalized poloidal flux. The density decay can be modified in order to fit as best as possible the experimental data [10]. The version of AORSA used in the numerical simulations presented here has a rectangular boundary which differs from the vacuum vessel structures adopted in [10]. In this paper we analyze primarily NSTX shot 130608. Figure 1 shows the electron density at the mid-plane and the insert figure shows the exponential density profiles in the SOL for three different values of n_{ant}.

Figure 2 shows the wave electric field amplitude obtained by the 2D full wave code AORSA for a single (dominant) toroidal mode, $n_\phi = -21$, which corresponds to an antenna phase of $-150°$ in (a) and for $n_\phi = -12$, which corresponds to an antenna phase of $-90°$, in (b), for NSTX discharge 130608 [4, 10, 13]. The wave frequency is $f = 30$ MHz. Six different cases of the electron density, n_{ant}, in front of the antenna (indicated in white) are plotted for both antenna phases together with the contour (in white) corresponding to the right hand cut-off in the cold plasma approximation, namely [14],

$$\frac{c^2}{\omega^2} k_\parallel^2 - \mathcal{R} = 0, \tag{1}$$

where $k_\parallel \approx k_z b_z = (n_\phi / R) b_z$ is the parallel (to the magnetic field) component of the refractive index (k_z and $b_z = B_z/|\boldsymbol{B}|$ are the toroidal component of the magnetic field and the toroidal direction of the magnetic field, respectively) and $\mathcal{R}$ is a component of the dielectric tensor for a cold plasma in the Stix's notation [14]. In figure 2, the black curves indicate the LCFS. From this figure we can clearly see that as soon as the density in front of the antenna increases sufficiently to 'open' the FW cut-off in front of the antenna, the wave electric field amplitude in the SOL increases strongly. In other words, these

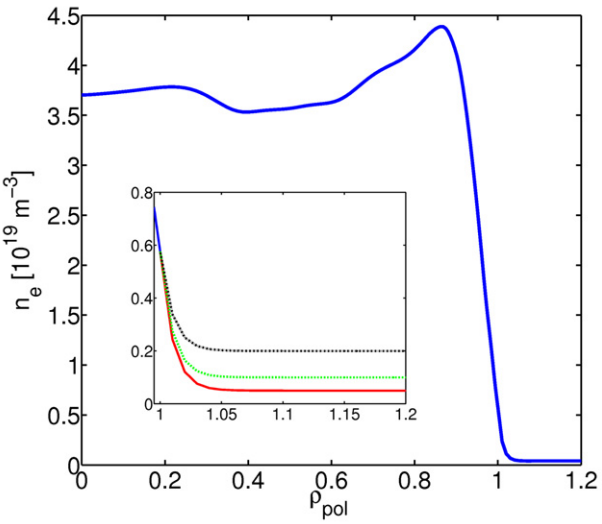

Figure 1. Electron density, n_e, as a function of the square root of the normalized poloidal flux, ρ_{pol}, for NSTX shot 130608 used in the numerical simulations presented here. The insert figure shows a closer view of the exponential decay of the density profile in the SOL for three different values of the density in front of the antenna: $n_{ant} = 0.5 \times 10^{18}$, 1.0×10^{18}, and 2.0×10^{18} m^{-3}.

simulations show a strong correlation between the location of the FW cut-off layer with the large electric field amplitude: when the FWs are no longer cut-off in front of the antenna and instead are propagating, the electric field amplitude outside of the LCFS increases. When the FW cut-off is 'closed' in front of the antenna and the waves are evanescent, the RF field amplitude in the SOL remains small. It is also important to note that for very low density, the RF field is strongly peaked radially and localized in front of the antenna, because the wave is strongly evanescent. For high density, when the wave is propagating, standing waves appear to form outside of LCFS independent of the launched wavenumber selected. In fact, these results appear for both antenna phases shown. Furthermore, it appears that with increasing density, the RF field amplitude in the SOL increases but not monotonically. The above effects are more evident for $n_\phi = -12$ (figure 2(b)). Finally, it is important to mention that, in the simulations shown in figure 2, no SOL power losses are found considering as absorption mechanisms, throughout the plasma, the 'standard' kinetic effects (Landau damping and transit-time magnetic pumping) retained in the hot plasma dielectric tensor. An analysis on the SOL power losses is presented in the section 2.2.

2.1. Analysis of the electric field in the SOL

In these numerical simulations shown in the previous subsection we found that, when the wave is propagating in the SOL, a standing wave can form outside of LCFS. Here, a 2D model is derived to verify the existence of these modes in the SOL for the specific parameters adopted in the numerical simulations. The starting point is the homogeneous wave equation

$$\nabla(\nabla \cdot \boldsymbol{E}) - \nabla^2 \boldsymbol{E} - \frac{\omega^2}{c^2} \varepsilon \cdot \boldsymbol{E} = 0 \tag{2}$$

where $\boldsymbol{E}$ is the electric field and $\varepsilon_{ij} = (\delta_{ij} - \hat{b}_i \hat{b}_j)\mathcal{S} + \hat{b}_i \hat{b}_j \mathcal{P} - i\epsilon_{ijk} \hat{b}_k \mathcal{D}$ is the dielectric tensor with $\hat{\boldsymbol{b}} = \boldsymbol{B}/|\boldsymbol{B}|$ the unit vector

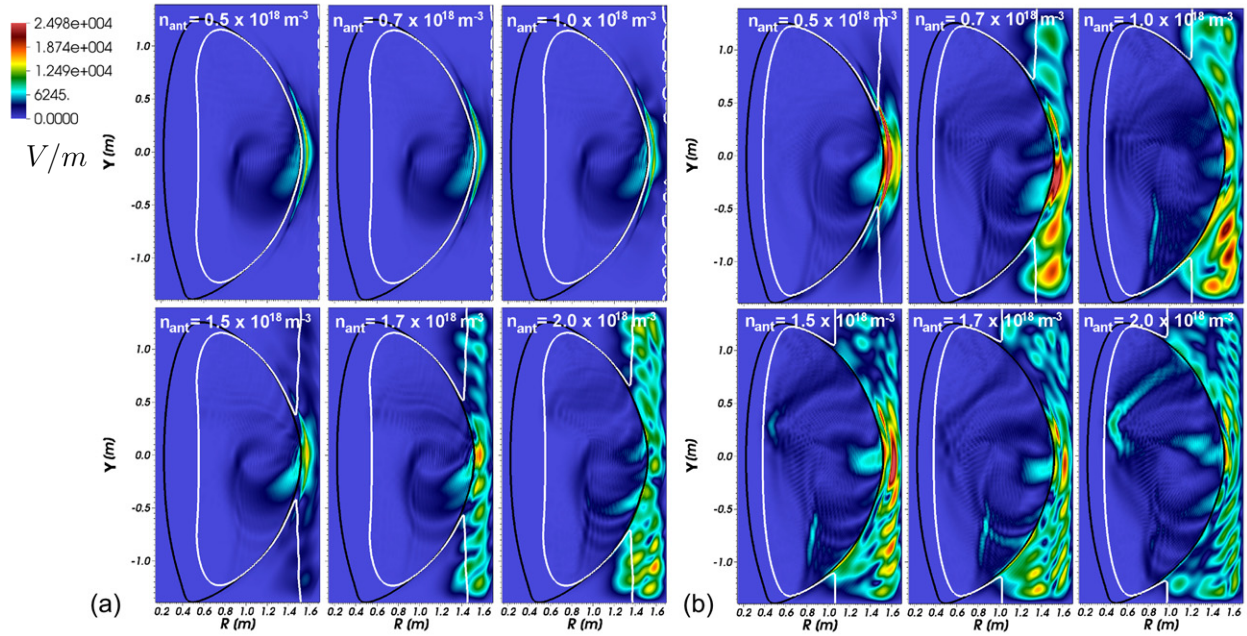

Figure 2. Electric field amplitude for different density values in front of the antenna ($n_{\rm ant}$) (shown in the plots) with toroidal mode numbers $n_\phi = -21$ (a) and $n_\phi = -12$ (b). The white and black curves indicate the FW cut-off layer and the LCFS, respectively.

of the magnetic field and $\mathcal{S}$, $\mathcal{P}$, and $\mathcal{D}$ the components of the dielectric tensor for a cold plasma in the Stix's notation [14].

Applying the following assumptions:

- the electric field in the form $E \sim \exp(i\boldsymbol{k}\cdot\boldsymbol{r})$, where $\boldsymbol{k}$ and $\boldsymbol{r}$ are the wave and the position vector, respectively;
- the refractive index, $\boldsymbol{N} \equiv c\boldsymbol{k}/\omega$, in the form

$$\boldsymbol{N} = \frac{c}{\omega}\left(\frac{\pi}{L_x}\hat{\boldsymbol{x}} + k_y\hat{\boldsymbol{y}} + \frac{n_\phi}{R_{\rm ant}}\hat{\boldsymbol{z}}\right) \tag{3}$$

  where the radial component of $\boldsymbol{k}$ is assumed π/L_x with L_x the distance between the right vertical boundary and the cut-off layer (white curve) shown in figure 2; k_y is the vertical component of the wave vector, and the toroidal component of $\boldsymbol{k}$ is $n_\phi/R_{\rm ant}$ with n_ϕ the toroidal mode number used in the AORSA simulations, and $R_{\rm ant} \simeq 157$ cm is the radial location of the antenna. Equation (3) is introduced in order to verify the structures of the electric field in the SOL found in AORSA simulations (see figure 2). In other words, for the given parameters obtained by AORSA simulations, we want to verify the existence of propagating modes in the SOL, i.e., real values of k_y.
- a general direction of the magnetic field in order to take into account the poloidal component of the magnetic field, which is not negligible in NSTX. More specifically, we introduce a new vector basis such as $\hat{e}_1 = \hat{\boldsymbol{b}}$, $\hat{e}_2 = \hat{\boldsymbol{x}} \times \hat{\boldsymbol{b}}/|\hat{\boldsymbol{x}} \times \hat{\boldsymbol{b}}|$, and $\hat{e}_3 = \hat{e}_1 \times \hat{e}_2$;

one can solve the following dispersion equation

$$[N^2 - (\hat{\mathbf{e}}_2 \cdot \boldsymbol{N})^2 - S][N^2 - (\hat{e}_3 \cdot \boldsymbol{N})^2 - S] - [D^2 + (\hat{e}_2 \cdot \boldsymbol{N})^2(\hat{e}_3 \cdot \boldsymbol{N})^2] = 0 \tag{4}$$

where we have neglected the electric field component parallel to the magnetic field, i.e., $E_1 = 0$ (in AORSA simulations, this component is significantly smaller than the other two components), reducing the model to a 2D model. By using NSTX plasma parameters adopted in AORSA simulations we have found real values of k_y (namely, propagation modes in the vertical direction) which satisfied equation (4) and are comparable to the modes observed in figure 2 for a range of values of the magnitude and the direction of magnetic field in NSTX SOL region. Table 1 shows k_y values obtained solving equation (4) for two density values of each antenna phase shown in figure 2. In this evaluation $B = 0.33$ T, which is an average of the magnitude of the magnetic field in the SOL and $\chi = 25^\circ$ and $\phi = 240^\circ$, which are an average of the direction of the magnetic field in the SOL (below the mid-plane). χ and ϕ are the pitch angle and the angle in the $\hat{\boldsymbol{x}} - \hat{\boldsymbol{y}}$ plane, respectively. From table 1, one can also note that this 2D model captures the trend of k_y with respect to the density and the antenna phases. Furthermore, from this model it is found that the poloidal components of the magnetic field can play an important role in order to obtain the vertical modes in the SOL as shown in figure 2. In fact, for a purely toroidal magnetic field, namely $\chi = 0$, there is no a real k_y which can satisfy equation (4). Further and more quantitative studies for different machines will be presented in a future work.

2.2. Analysis of the SOL power losses

In order to understand whether the large wave electric field amplitude is one of the main drivers of the SOL power losses found in the NSTX experiments, we have inserted into AORSA an artificial 'collisional' damping mechanism as a proxy to represent the actual mechanism(s) which is(are) presently unknown [15]. A collisional frequency, ν, has been

Table 1. Values of k_y which satisfied equation (4) for given antenna phase (n_ϕ), density ($n_{e,ant}$), L_x, magnitude ($B = 0.33$ T) and direction ($\chi = 25^\circ$ and $\phi = 240^\circ$) of the magnetic field in the SOL.

n_ϕ	$n_{e,ant}$ ($\times 10^{18}$ m^{-3})	L_x (cm)	k_y (cm^{-1})	$\lambda_y \equiv 2\pi/k_y$ (cm)
21	1.7	~25	~0.34	~18.5
21	2.0	~32	~0.37	~17.0
12	0.7	~35	~0.20	~31.4
12	1.0	~48	~0.24	~26.2

implemented as the imaginary part of the angular frequency, ω, in the argument of the Plasma Dispersion function, Z:

$$Z\left(\frac{\omega - n\omega_c}{k_\parallel v_{th}}\right) \longrightarrow Z\left(\frac{\omega - n\omega_c + i\nu}{k_\parallel v_{th}}\right), \qquad (5)$$

where n is the harmonic number, ω_c is the cyclotron frequency, $k_\parallel$ is the parallel (to the magnetic field) component of the wave vector, and v_{th} is the thermal velocity. The term ν/ω is then an AORSA input parameter and allows us to adopt this specific proxy for a commensurate prediction of the power losses in the SOL region and, in particular, their behaviour as a function of the density in front of the antenna. It is important to note that without an added damping mechanism, such as this proxy in the SOL, no significant SOL power losses are predicted in the simulations, even in the presence of a large electric field amplitude (as shown in figure 2). Figure 3 shows the predicted absorbed power in the SOL region (SOL power losses) as a function of the density in front of the antenna (n_{ant}) assuming $\nu/\omega = 0.01$. Two different antenna phases are shown: $n_\phi = -12$ (dashed curve) and -21 (solid curve). As mentioned above, the cut-off of the fast wave corresponds to the right hand cut-off, see equation (1). In the HHFW frequency range, since the wave frequency is much higher than the local fundamental ion cyclotron frequency and much lower than the local lower hybrid frequency, the FW cut-off density can be written as [2, 3]

$$n_{e,FWcut-off} \propto \frac{k_\parallel^2 B}{\omega}, \qquad (6)$$

where B is the equilibrium magnetic field. The vertical line in figure 3, for both cases, represents the density at which the cut-off starts to be 'open' in front of the antenna, i.e., when the wave is propagating in front of the antenna and the amplitude of the electric field starts to increase in the SOL region, as shown in figure 1. From figure 3 one can note a rapid transition in the fraction of the power lost to the SOL from the evanescent region to the propagating region both for $n_\phi = -12$ and -21. Moreover, for lower n_ϕ ($n_\phi/R = k_\phi \sim k_\parallel$) the transition occurs at lower n_{ant} as expected from equation (6). When the cut-off is 'closed' in front of the antenna and the wave is evanescent, with a small SOL RF field amplitude, the fraction of power lost to the SOL is found to be smaller with respect to the regime in which the cut-off is 'open' and the wave propagating in the SOL has a large RF field amplitude. For very low density the RF power losses tend to increase again with decreasing density, due to the fact that the wave is so strongly evanescent that the power can be only damped in front of the antenna, consistent with the large electric field localized in front of the antenna as indicated in figure 2. This effect is more evident

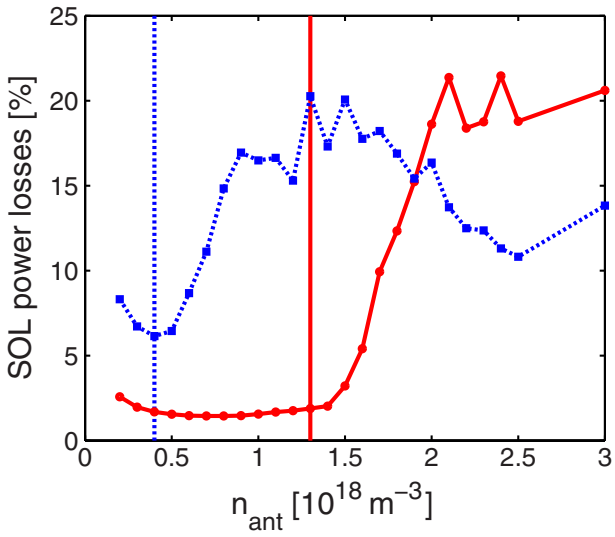

Figure 3. Fraction of power lost to the SOL as a function of the density in front of the antenna for $n_\phi = -21$ (solid curve) and $n_\phi = -12$ (dashed curve). The vertical lines represent the value of the density for which the FW cut-off starts to be 'open' in front of the antenna (see figure 2).

for the $n_\phi = -12$ than $n_\phi = -21$ because of the significant shift of the FW cut-off density toward lower density and, as a consequence, a narrower density range for the evanescent region. It is also important to mention that in the density range adopted in these simulations the slow wave is found to be cut-off. As a further confirmation of these results, we did the same numerical analysis (not shown) for another independent NSTX discharge, 130621, and the same edge loss transitions have been found.

Power deposition in the SOL has also been evaluated in 3D using 81 toroidal modes to reconstruct the full antenna spectrum. Figure 4 shows the 3D absorbed power deposition in the SOL for $n_{ant} = 2.5 \times 10^{18}$ m^{-3} and three different ρ slices (ρ is the square root of the normalized poloidal flux): $\rho = 1.1$ to 1.15, near the antenna in figure 4(a), $\rho = 1.05$ to 1.1 in figure 4(b), $\rho = 1$ to 1.05, near the LCFS in figure 4(c) (the antenna is at $\rho \simeq 1.15$). The NSTX discharge analyzed is 130608 assuming $\nu/\omega = 0.01$. From these figures it appears that (i) the SOL power losses are larger near the antenna (see figure 4(a)), and near the LCFS (see figure 4(c)) consistent with the experimental studies (see figures 11 and 12 of [6]) (the flux surface average of the absorbed power is about 1.75×10^4 W m^{-3} at $\rho = 1.15$ (at the antenna location), 0.8×10^4 W m^{-3} at $\rho = 1.05$, and 1.35×10^4 W m^{-3} at $\rho = 1$ (at the LCFS)); and (ii) large SOL power losses below the mid-plane due to the large RF field.

We can now extend our numerical analysis to the NSTX-U experiment, which will be operating at the end of 2014 [16], in order to make some predictions on the behaviour of the RF power losses in future NSTX-U discharges. We analyze an H-mode scenario being considered for NSTX-U with $B_T = 1$ T, obtained by using the TRANSP code [17]. This toroidal magnetic field corresponds to the full toroidal magnetic field that will be available for the NSTX-U experiment. Figure 5 shows the predicted RF power losses in the SOL as a function of n_{ant} for this NSTX-U case. Exactly the

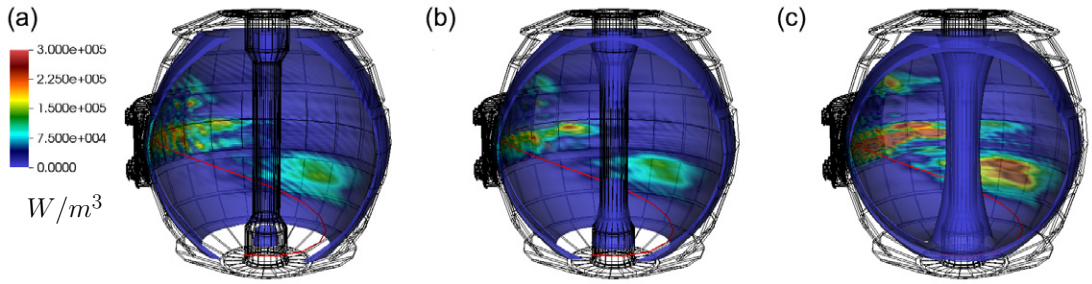

Figure 4. 3D contour plots of the absorbed power in the SOL for three different ρ slices: (*a*) $\rho = 1.1$ to 1.15 (near the antenna located at $\rho \simeq 1.15$), (*b*) $\rho = 1.05$ to 1.1, and (*c*) $\rho = 1$ to 1.05 (near the LCFS). The density in front of the antenna is $n_{\rm ant} = 2.5 \times 10^{18}$ m$^{-}3$ (assuming $\nu/\omega = 0.01$). The red curve represents a magnetic field line starting from the antenna and shows the large pitch angle of the magnetic field with respect to the antenna.

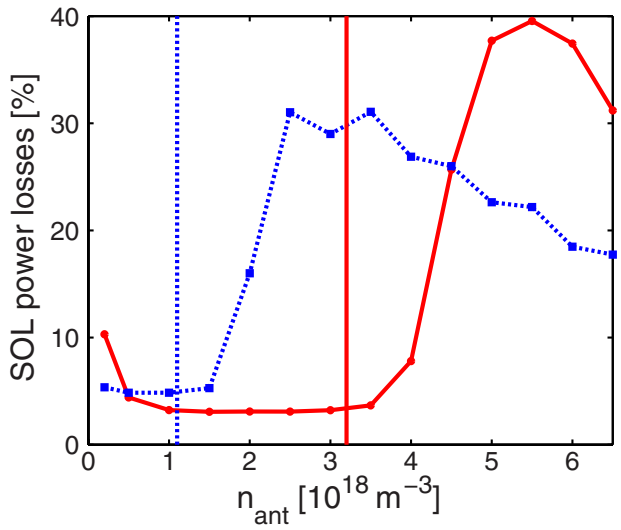

Figure 5. Fraction of power lost to the SOL as a function of the density in front of the antenna for $n_\phi = -21$ (solid curve) and $n_\phi = -12$ (dashed curve), for an NSTX-U case with $B_{\rm T} = 1$ T. The vertical lines represent the value of the density for which the FW cut-off starts to be 'open' in front of the antenna.

same transition behaviour found in the NSTX case is predicted for the NSTX-U case for both $n_\phi = -21$ (solid curve) and $n_\phi = -12$ (dashed curve). The main important difference with respect to the NSTX case is that the transition to higher losses in the SOL occurs at higher density. This is explained by the fact that the FW cut-off is proportional to the magnetic field (see equation (6)), and therefore for the NSTX-U case with $B_{\rm T} = 1$ T the transition occurs for about a factor of two higher in density with respect to NSTX case with $B_{\rm T} = 0.55$ T (compare vertical lines in figures 3 and 5 for each n_ϕ). This result tells us that the evanescent region for NSTX-U, in which the SOL power losses are smaller, will be wider than the one in NSTX and therefore from the experimental point of view there will be a wider SOL density range in which the experiment can run with lower SOL power losses.

3. Conclusions

The results shown in this paper might appear to be counter-intuitive in the sense that for low density in front of the antenna the wave is evanescent and, in principle, the antenna-plasma coupling is relatively poor; and vice-versa, for high density the wave is propagating and the antenna-plasma coupling is relatively good. However, with these simulations we have demonstrated that too high density in front of the antenna, although positive for the antenna-plasma coupling, leads to substantial increases of the RF electric field in the SOL and corresponding RF power losses. As a result, from the experimental point of view, it is crucial to be able to optimize the density in SOL region in order to balance the antenna coupling and the RF power losses in the SOL. For the NSTX-U experiment, this optimization will be more easily facilitated with respect to NSTX due to the fact that, with higher magnetic field, the transition between the evanescent and the propagating region will be at a higher density $n_{\rm ant}$ since the cut-off density value is directly proportional to the magnetic field. These results suggest that SOL power losses such as predicted here, may also prove to be important for ICRF heating on ITER. Though, it is important to note that ITER will employ minority ion cyclotron heating with excitation in the range of the third harmonic of the deuterium ion cyclotron frequency, a much lower value than the $\sim 11^{\rm th}/12^{\rm th}$ harmonic excited on NSTX. Some insight into the effect of reducing the harmonic value will be obtained on NSTX-U, for which excitation will be at the $\sim 5^{\rm th}/6^{\rm th}$ harmonic. Also, the geometry and the main plasma parameters are very different on ITER with respect to the NSTX and NSTX-U experiments; e.g., the considerably smaller pitch of the magnetic field on ITER and its larger size combine to make the field line length from the lower to upper divertor strike points much greater on ITER than NSTX/NSTX-U. Therefore, in order to develop conclusive predictions for ITER, further studies, from both the experimental and theoretical point of view, are necessary in order to identify the actual physical mechanism(s) behind the RF power losses in NSTX. Nevertheless, the optimization of the density in the SOL region could prove to be crucial for the performance of the ICRF heating system in ITER since the distance between wall and separatrix is large ($\sim$20 cm).

Acknowledgments

This work was supported by the SciDAC Center for Wave-Plasma Interactions under DE-FC02-01ER54648 and the US DOE under DE-AC02-CH0911466.

References

[1] Ono M. *et al* 2000 *Nucl. Fusion* **40** 557
[2] Hosea J.C. *et al* 2008 *Phys. Plasmas* **15** 056104
[3] Phillips C.K. *et al* 2009 *Nucl. Fusion* **49** 075015
[4] Taylor G. *et al* 2010 *Phys. Plasmas* **17** 056114
[5] Perkins R.J. *et al* 2012 *Phys. Rev. Lett.* **109** 045001
[6] Perkins R.J. *et al* 2013 *Nucl. Fusion* **53** 083025
[7] Wukitch S.J. *et al* 2007 *AIP Conf. Proc.* **933** 75
[8] Jacquet P. *et al* 2011 *Nucl. Fusion* **51** 103018
[9] Jaeger E.F. *et al* 2001 *Phys. Plasmas* **8** 1573
[10] Green D.L. *et al* 2011 *Phys. Rev. Lett.* **107** 145001
[11] Wilson J.R. *et al* 2005 *AIP Conf. Proc.* **787** 66
[12] Myra J.R. *et al* 2006 *Nucl. Fusion* **46** S455
[13] Hosea J.C. *et al* 2009 *AIP Conf. Proc.* **1187** 105
[14] Stix T.H. 1992 *Waves in Plasmas* (New York: American Institute of Physics)
[15] Bertelli N. *et al* 2014 *AIP Conf. Proc.* **1580** 310
[16] Menard J.E. *et al* 2012 *Nucl. Fusion* **52** 083015
[17] Gerhardt S.P., Andre R. and Menard J.E. 2012 *Nucl. Fusion* **52** 083020